## RESEARCH ARTICLE

# Farmland Aerial Images Fast-Stitching Method and Application Based on Improved SIFT Algorithm

**YUANYUAN LIU[1,2], MING HE[1], YUEYONG WANG[3], YU SUN[1], AND XUEBING GAO[1]**

[1]College of Information Technology, Jilin Agricultural University, Changchun, Jilin 130118, China
[2]Department of Biosystems and Agricultural Engineering, Oklahoma State University, Stillwater, OK 74078, USA
[3]College of Engineering and Technology, Jilin Agricultural University, Changchun, Jilin 130118, China

Corresponding author: Yueyong Wang (yueyongw@jlau.edu.cn)

**ABSTRACT** The main black land conservation measure in China is the straw return to the fields. The processing of high-resolution images collected by aerial photography of UAVs through image stitching technology can provide image information for achieving fast and accurate detection of straw cover over large areas. The classical SIFT algorithm has many drawbacks, such as high dimensionality of feature descriptors, high computational effort, and low matching efficiency. To solve the problems above, this study proposes an improved algorithm. First, the method down sampled the high-resolution images before detecting the features to reduce the number of feature points and improve the efficiency of feature detection. Then, matching among feature points is achieved by gradient normalization-based feature descriptors to improve the matching accuracy. Next, the Progressive Sample Consistency algorithm eliminates the mismatch points and optimizes the transformation model. Finally, the images are fused with optimal stitching combined with fade-in and fade-out to achieve high-quality stitching. The comparative experimental results show that compared with the traditional SIFT and the speed-up robust feature algorithms, the algorithm has the advantage of the speed and good robustness to angle rotation, and makes full use of the texture information and the detail information, so it has higher accuracy. Compared with the traditional methods, the panoramic stitching image quality herein is excellent and can be applied to subsequent straw cover detection, the straw cover error is ≤3%, meeting the demand for large-area straw cover detection. Overall, the method proposed herein achieves an ideal balance between accuracy and efficiency; and outperforms other widely used and superior methods.

**INDEX TERMS** Aerial images, down sampling, SIFT operator, panoramic stitching, straw coverage rate.

## I. INTRODUCTION

In recent years, UAV remote sensing technology has become increasingly popular due to its speed, ease of operation, and flexibility [1]. Aerial images and videos captured by UAVs are widely utilized in various fields, such as agriculture monitoring [2], weather forecasting [3], [4], and geographic mapping [5]. Agriculture is the first area where remote sensing

The associate editor coordinating the review of this manuscript and approving it for publication was Miaohui Wang.

technology has been applied and the benefits are significant [6]. Agricultural remote sensing monitoring mainly takes crops and soil as the objects; and uses the spectral characteristics of the ground to monitor crop growth, crop quality, crop pests, and diseases. Precision agriculture technologies, represented by artificial intelligence (AI) and machine learning (ML) technologies, are now making a huge contribution to agricultural production [7]. AI and machine learning improve crop yield prediction with real-time sensor data from drones and visual analytics data. Agriculture has also become one of

the most promising AI and ML application scenarios. Blackland resources are very scarce worldwide, and the only four major Blackland areas are the Ukrainian plains in Ukraine, the Mississippi plains in the United States, the Northeast plains in China, and the Pampas in South America from Argentina to Uruguay. In the northeastern plains of China, corn and rice are the main crops. Therefore, the main black land conservation measure in China is the straw return to the fields, and relevant straw return subsidy policies have been promulgated to more effectively limit straw burning and guide farmers to return straw to the fields in a reasonable manner [8]. The question of how to quickly and accurately assess quantitatively the straw return rate is very important. It is difficult to calculate the coverage rate at any time because of the wide crop cultivation area, so it is possible to obtain the image information by collecting high-resolution images through aerial photography by UAV. However, the single image collected incompletely covers the target area due to the height and camera resolution limitations. Therefore, stitching multiple images collected by UAV aerial photography to generate a large-area and high-resolution panoramic image is the key to improving the efficiency and accuracy of straw cover detection.

Image stitching is the process of combining multiple overlapping images to compose a high-resolution panoramic image. Image alignment is the key technology for UAV aerial image stitching. Scholars worldwide have conducted several studies on this technology. Lowe *et al.* [9] proposed a scale-invariant feature transform (SIFT) algorithm that has the advantages of high matching accuracy, good scale invariance, and strong robustness to illumination and viewpoint changes. However, the matching is time-consuming and challenging to meet the requirements of fast-stitching processing. Hou *et al.* [10] improved the high-dimensionality problem for feature vectors detected by the SIFT algorithm and proposed a scale-invariant feature transformation based on cyclic descriptors to improve the efficiency of coarse matching of feature points. Bay *et al.* [11] proposed a highly robust local feature point detection algorithm, the speed-up robust feature (SURF) algorithm. It improved the interest point extraction and feature vector description methods and the speed of feature extraction and matching compared to the SIFT algorithm. However, the number of matching points is reduced and less tolerant of scale and rotational changes. Hu *et al.* [12] used the SURF algorithm to stitch aerial images from UAVs and found that it is faster at matching images than the SIFT algorithm. However, the number of matching points is small and unevenly distributed, and the image-stitching quality is low. Previous studies on image stitching have focused on the simple case of stitching two images [13] or multiple images located on the same row to generate panoramic images [14], [15]. Presently, researchers worldwide have less research on the fast stitching of multiple high-resolution images. The problem with the traditional stitching of multiple images is that there are rotation angles between the acquired high-resolution images, which makes image alignment difficult

and time-consuming. At the same time, the errors generated by multi-image stitching cumulatively affect the accuracy of panoramic stitching images [16], [17], [18].

To address these problems, a fast-stitching technique was proposed for straw farmland images based on the optimized SIFT algorithm. Compared to the traditional SIFT algorithm [8], the image is down sampled before feature detection to reduce the number of feature points and improve the efficiency of feature extraction. MN-SIFT feature descriptor is used for matching, which has better texture features and can improve the matching accuracy. Here the original coordinates and scale parameters of feature points are restored in the feature matching stage, and feature point matching is performed according to the similarity metric to ensure excellent image-stitching quality and accuracy. Based on this, the Progressive sample consistency (PROSAC) algorithm eliminates false matches, improves the accuracy of matching feature points, and solves the projection transformation matrix model using the least-squares method. To eliminate the image misalignment, ghosting, and even stitching gaps generated during stitching, the modified optimal stitching line and fading-in and fading-out method are used to fuse the images, which completes the smooth transition between the overlapping image regions and the nonoverlapping stacked domain and enhances the details of the images. A layered stitching strategy is designed for multiple high-resolution images, which reduces the accumulated error of continuous projection and improves the accuracy and stitching efficiency of image stitching compared with the traditional method. Finally, the fast stitching of multiple remote sensing images of straw farmland is realized, and a high-quality panoramic image with reference value was generated.

## II. PROPOSED METHOD

### A. FAST STITCHING ALGORITHM

Presently, the framework of remote sensing image-stitching algorithms has been perfected. It is the primary research focus on studying the fast-stitching algorithm of remote sensing images and its adaptability and robustness to different scenes [19], [20], [21]. The panoramic stitching method of remote sensing images of straw farmlands is studied through low-altitude and high-resolution sequence images collected by the UAV, as shown in Figure 1. Herein, a fast-stitching method is proposed for high-resolution images in fields to solve the low-feature alignment efficiency problem due to the high resolution of field images and the similar color of the straw surface. Figure 2 shows the overall flow of our method. The main contributions of the improved image stitching method proposed herein are summarized as follows: first, histogram equalization and denoising are preprocessed on the UAV aerial photography sequence photographs of the straw farm. Second, the optimized SIFT algorithm detects the feature points of the processed image to obtain the feature point descriptor MN-SIFT [22], and feature point matching is performed. Next, the PROSAC algorithm rejects false matches and improves the matching accuracy. Finally, the stitching

area is computed using the image projection transformation model, and the best stitching line and fade-in and fade-out techniques fuse the images and enhance the image quality. Multi-image stitching generates large-area panoramic images according to the multi-image-stitching strategy, which provides a scientific reference for large-area straw coverage detection and geographic information detection.
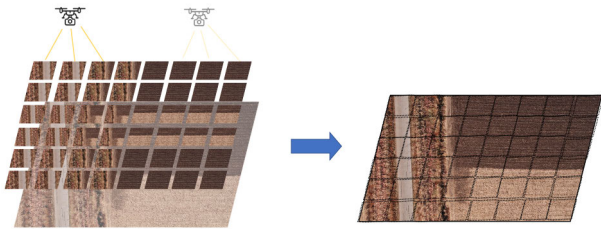


**FIGURE 1.** Schematic diagram of aerial photography acquisition.
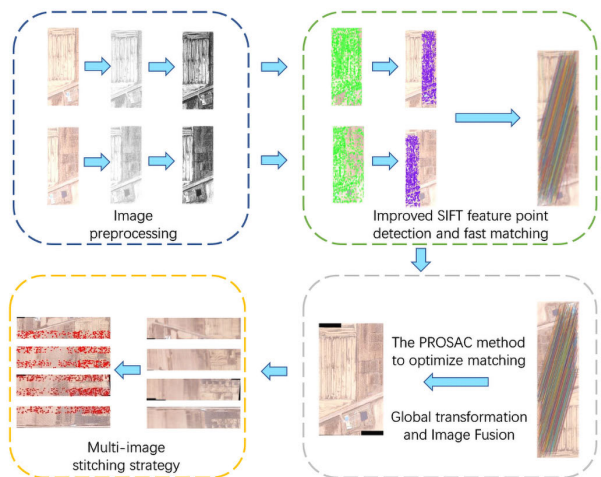


**FIGURE 2.** Overall flow chart of fast stitching method.

## B. IMAGE ALIGNMENT

### 1) FEATURE POINT EXTRACTION

It is challenging to match the texture, projection, luminosity, and nonlinear intensity variations in the high-resolution aerial images of farmlands taken by UAVs because the straw features and colors are similar and the images are taken at different times from different viewpoints. To find and match feature points, the conventional SIFT algorithm is used directly, which has drawbacks, such as feature point duplication, high time consumption, and poor alignment efficiency. The improved SIFT algorithm which has better stability and invariance, preferentially down samples the image before feature detection to effectively reduce the number of feature points and improve the alignment accuracy. Also, a new feature descriptor is introduced, which describes the textural features of the image better and enhances the alignment efficiency effectively. The process of the improved SIFT algorithm is outlined below as follows:

• **Image down sampling:** According to the down sampling factor (k), the number of image sampling points is reduced, and each row and column of the input map is sampled at k point intervals to form the resulting map; thus, reducing the image resolution and improving the efficiency of matching feature point detection, as shown in Figure 3. As the information quality contained in remote sensing images in different scenes varies, k also varies. Herein, k = 5, which was selected after several experiments by combining the information of the straw farmland images.
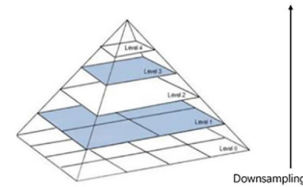


**FIGURE 3.** Flow chart of down sampling.

• **Scale-space extreme value point detection:** Scale-space extreme value point detection: This step entails extreme point detection and the search for image locations on all scales. Potential points of interest that are invariant to scale and rotation are identified using Gaussian differential functions. The scale-space of a two-dimensional image L(x, y, $\sigma$) is defined as the convolution of the scale-variable Gaussian function G(x, y, $\sigma$) with the original image I(x,y), as follows:

$$G(x, y, \sigma) = \frac{1}{2\pi\sigma^2} e^{-(x^2+y^2)/2\sigma^2} \tag{1}$$

$$L(x, y, \sigma) = I(x, y) * G(x, y, \sigma) \tag{2}$$

• **Feature point pinpointing:** A three-dimensional quadratic function is fitted to accurately determine the location and scale of feature points. Also, low-contrast feature points and unstable edge response points are filtered to enhance the matching stability and improve noise immunity.

• **Feature point descriptor generation:** This study focuses on farmland images with distinct textural characteristics, and different plots have different textural complexities. Therefore, a gradient normalization-based MN-SIFT [22] descriptor is used, which better describes textural features, better robustness to farmland remote sensing images, and can improve the matching efficiency. It modifies gradient magnitudes to obtain continuous-valued magnitude features($\bar{\Omega}$)as follows:

$$\bar{\Omega}(x, y) = \frac{\Omega(x, y) - \Omega_{min}}{\Omega_{max} - \Omega_{min}} \tag{3}$$

Using the feature points as the origin, an image region H(x,y) of size 41piex $\times$ 41piex is constructed, and then H(x,y) is divided into 4 $\times$ 4 subregions as shown in Figure 4. As shown in (3), where $\Omega_{min}$ and $\Omega_{max}$ are the minima and maximum values of the gradient amplitude obtained from the image region, and (x,y) denotes the pixel position.

The region H(x,y) is convolved with $[-1,0,1]$ and $[-1, 0, 1]^T$ kernels to obtain image gradients in the
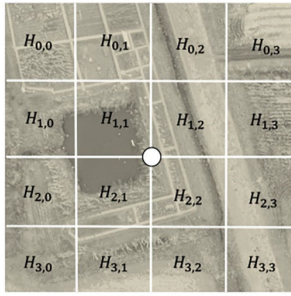
**FIGURE 4.** Image area map.

horizontal (Fh) and vertical (Fv) directions, respectively. Then the gradient magnitudes($\Omega$)and directions($\beta$)are calculated as follows:

$$\Omega(x, y) = \sqrt{F_h(x, y)^2 + F_v(x, y)^2} \quad (4)$$

$$\beta(x, y) = atan2(F_v(x, y), F_h(x, y)) \quad (5)$$

As shown in Figure 4, each subregion is denoted by $H_{r,c}$(r = 0,1,2,3;c = 0,1,2,3), the set of pixels in each subregion is {H(x, y) : $x \in [l_c, u_c] \wedge y \in [l_r, u_r]$}, as follows:

$$l_c = \frac{(41 - 1)c}{4}; \quad u_c = \frac{(41 - 1)(c + 1)}{4} \quad (6)$$

$$l_r = \frac{(41 - 1)r}{4}; \quad u_r = \frac{(41 - 1)(r + 1)}{4} \quad (7)$$

Dividing the direction $\beta(x, y)$ into 8 levels by taking the remainder operation, and calculating the feature histogram $h_{r,c,t}$, as follows:

$$L(x, y) = mod(\left\lfloor \frac{\beta(x, y)}{\frac{2\pi}{8}} + \frac{1}{2} \right\rfloor, 8) \quad (8)$$

$$h_{r,c,t} = \sum_{x=l_c}^{u_c} \sum_{y=l_r}^{u_r} \bar{\Omega}(x, y)\delta(L(x, y) = t) \quad (9)$$

where, $t \in [0, 7]$, $\delta$ function takes values equal to zero at all points except zero, its value $\delta(z)$ is as follows:

$$\delta(z) = \begin{cases} 1 & \text{the main direction} \\ 0 & \text{other directions} \end{cases} \quad (10)$$

Finally, the $h_{r,c,t}$ of each subregion histograms are concatenated over all $H_{r,c}$, generating a feature descriptor MN-SIFT [22] that is independent of scale, rotation, illumination, etc.

The consumption and low matching efficiency of the traditional algorithm are improved. This improvement strengthens its robustness to straw image texture features and maintains its invariance to image rotation, scaling, brightness changes, and a certain degree of stability to viewpoint changes, affine transformations, and noise.

### 2) FEATURE POINT MATCHING

According to the feature point detection results, the feature point coordinates and scale parameters are restored to ensure the accuracy of subsequent high-resolution image stitching.

Afterward, the MN-SIFT [22] descriptor of the feature points measures the similarity, and the matched pairs are extracted. The similarity measure evaluates the similarity of two feature points, and the Euclidean distance between the feature points is generally used as a criterion to filter the matches. Next, the Euclidean geometric distance is calculated from a feature point to the corresponding feature point of another image, as shown in (11), and the two feature points in which the Euclidean geometric distance is the smallest and the second smallest only are selected. Furthermore, the ratio (r) of the Euclidean geometric distances of the two selected feature points is calculated. If r is ≤a specific threshold T (the threshold is usually between 0.4 and 0.6), the pair of matches is recognized; otherwise, it is rejected.

$$D(p, q) = ||D_p - D_q|| = \sqrt{\sum_{i=1}^{n} (D_p[i] - D_q[i])^2} \quad (11)$$

where p is a feature point in the reference image, q is a feature point in the target image, $D_p$ and $D_q$ are the n−dimensional feature descriptors of p and q.

The feature point matching is a problem of similarity retrieval between high-dimensional vectors by distance functions. The Best-Bin-First(BBF)search algorithm establishes data indexes to achieve a fast search of high-dimensional data and fast matching. It can ensure the priority retrieval of the space with a higher probability of containing the nearest neighbors, which effectively reduces the computational complexity, increase the operation speed and improve the alignment efficiency. The method proposed herein enables fast matching of matching points and improves the overall stitching efficiency.

### C. PROSAC ALGORITHM FINE MATCHING

Although the fast matching of image feature points is achieved, the process inevitably produces some false matches. False matching pairs may lead to ghosting and misalignment in the subsequent stitched images, so matching results must be filtered to achieve fine matching of image feature points and reliable matching feature point pairs. Next, the PROSAC algorithm optimizes the matching results. It uses a similarity function to rank the quality of feature point pairs linearly, and only the sample set with the highest-ranked correspondence is gradually selected for model hypothesis and validation at a time. The details are as follows: Four sets of matching pairs are randomly drawn from the sample set, and the transformation matrix H (12) is calculated according to (13), denoted as model M. The projection error of all feature matching point pairs in the matching point set with the model M is calculated according to the error function (14), and if the requested error is less than a threshold value of 0.1, the matching point pair is added to the inner point set I until the end of the iterations when the number of iterations reaches a preset number (500 in this study). The optimal single-response matrix H is found according to the optimal inner

point set I.

$$H \begin{bmatrix} m_{11} & m_{12} & m_{13} \\ m_{21} & m_{22} & m_{23} \\ m_{31} & m_{32} & 1 \end{bmatrix} \tag{12}$$

$$\begin{cases} a' = \dfrac{m_{11}a + m_{12}b + m_{13}}{m_{31}a + m_{32}b + 1} \\ b' = \dfrac{m_{21}a + m_{22}b + m_{23}}{m_{31}a + m_{32}b + 1} \end{cases} \tag{13}$$

where (a,b) is the image pixel point coordinates before transformation matrix processing, (a', b') is the image pixel point coordinates after transformation matrix processing.

$$\sum_{i=0}^{n} (a'_i - \frac{m_{11}a_i + m_{12}b_i + m_{13}}{m_{31}a_i + m_{32}b_i + 1})^2$$
$$+ (b'_i - \frac{m_{21}a_i + m_{22}b_i + m_{23}}{m_{31}a_i + m_{32}b_i + 1}) \tag{14}$$

### D. IMAGE FUSION

Image fusion is the last image-stitching step, which is the key to high-quality image stitching. Straw farmland aerial images have a complex background and contain more information, including houses, roads, and other distractions in addition to the straw in the field. Besides, the stitching process is prone to image overlap, ghosting, and misalignment. To solve these problems, image fusion uses the modified optimal stitching line [23] and a fading-in and fading-out method. The basic idea of the optimal stitching line is dynamic planning, which is calculated by the energy function (15) to find the path with the minimum energy value. The method proposed herein incorporates color difference, gradient difference, and textural complexity to find the most similar sutures on both sides in the overlapping region. Also, the strategy of finding the optimal sutures greatly reduces the overlapping region; thus, alleviating the blurring and ghosting problems. The fading-in and fading-out method is a distance-based weighted average method. Its weights are selected according to the distance from the overlapping boundary. The closer the distance from the boundary, the smaller the weight value is taken; thus, reducing the influence of the edge of the overlapping region of the evidence and making a smooth transition to the fusion boundary. The two images to be fused are defined as $I_1$ and $I_2$ respectively, and the fused image is $I$ (16).

$$W = \frac{E_{Color} + E_{Texture} + \tau}{E_{Grad}} \tag{15}$$

where W is the final weight, $E_{Color}$ is a color difference item, $E_{Grad}$ is the gradient difference term, $E_{Texture}$ is the texture difference term, $\tau$ is a penalty item.

$$(x, y) = \begin{cases} I_1(x, y) & (x, y) \in I_1 \\ d_1(x, y) I_1(x, y) + d_2(x, y) I_2 & (x, y)(x, y) \\ & \in (I_1 \cap I_2) \\ I_2(x, y) & (x, y) \in I_2 \end{cases} \tag{16}$$

where $d_1(x, y)$ and $d_2(x, y)$ are the weight functions, $(x, y)$ is the distance from the boundary and $d_1(x, y) + d_2(x, y) = 1$.

The method proposed herein achieves a smooth transition between the overlapping regions and the nonoverlapping stacked domains of the image. Thus, this smooth transition improves the image quality and removes the redundant information in the overlapping regions of the image while supplementing the effective information in the nonoverlapping regions to enhance the image details and obtain a more comprehensive and clearly described stitched image.

### E. MULTIPLE HIGH-RESOLUTION-IMAGES PANORAMIC STITCHING

The traditional multi-image stitching method entails finding the projection models of all images in the stitching sequence and using a combination of multiple models to achieve panoramic stitching of multiple images [24], [25]. This method is simple to operate, but causes stitching errors to accumulate. For high-resolution aerial images, the stitching error causes serious misalignment of the stitched image and affects the panoramic image accuracy.

Herein, a layered stitching strategy of multiple high-resolution images was designed. The layering idea is such that because the relative position relationship between the images acquired from the same route is more accurate, the deflection angle and the error accumulated by the conversion model are smaller. Here, each layer of the image is primarily stitched. Next, the panoramic view of the result of each layer is stitched to form a complete panoramic image, as shown in Figure 5.
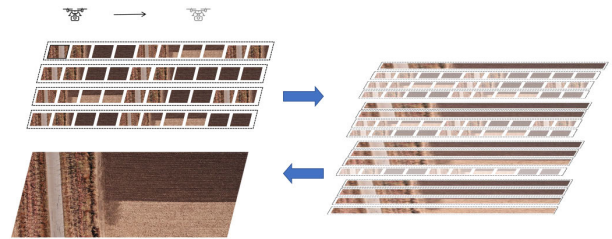


**FIGURE 5.** Stitching strategy diagram.

## III. EXPERIMENTS

### A. IMAGE ACQUISITION AND EXPERIMENTAL EQUIPMENT

The experimental images were collected from the conservation tillage experimental base of the Agricultural Machinery Research Institute in Changchun, Jilin Province, and the field experiment base of Jilin Agricultural University. The acquisition time was November 5, 2021, around 10:00 a.m. to 12:00 p.m. on a cloudy day. The experiment used a DJI M200 V2 UAV equipped with a stabilizing gimbal X5S to acquire images. In this study, the UAV acquired 120 meters of RGB images of different straw farmland with image overlap at 50% and an image size of 2970 × 5280 pixels. A total of 200 images were acquired for the study of stitching.

The experiments were performed on the Windows 10 system with an NVIDIA GeForce GTX 1050 GPU, 2.50 GHz

**TABLE 1.** k-value comparison results.

| Group Number | Parameters | 1 | 2 | 3 | 4 | 5 | 6 | 7 | 8 |
|---|---|---|---|---|---|---|---|---|---|
| 1 | feature number | 58201 | 26503 | 1 2623 | 8671 | **6026** | 2690 | 1386 | 863 |
| | Matching rate /% | 17 | 20 | 22 | 18 | **24** | 20 | 16 | 14 |
| | Time /s | 62.38 | 16.74 | 7.92 | 4.24 | **2.38** | 1.65 | 1.06 | 0.53 |
| 2 | feature number | 53637 | 30279 | 1 0643 | 8093 | **5036** | 2413 | 1186 | 654 |
| | Matching rate /% | 16 | 18 | 21 | 19 | **22** | 20 | 13 | 14 |
| | Time /s | 58.24 | 14.36 | 6.03 | 3.27 | **2.13** | 1.33 | 0.92 | 0.47 |
| 3 | feature number | 46255 | 19860 | 9672 | 7412 | **5532** | 2269 | 1237 | 771 |
| | Matching rate /% | 15 | 18 | 22 | 23 | **25** | 22 | 19 | 13 |
| | Time /s | 54.66 | 12.79 | 5.17 | 3.19 | **2.53** | 1.01 | 0.79 | 0.44 |
| 4 | feature number | 55371 | 28430 | 13795 | 9061 | **4863** | 2735 | 1542 | 996 |
| | Matching rate /% | 19 | 22 | 24 | 23 | **26** | 23 | 19 | 15 |
| | Time /s | 58.72 | 19.64 | 8.03 | 4.11 | **2.55** | 1.73 | 1.27 | 0.76 |
| 5 | feature number | 47623 | 19756 | 11632 | 7824 | **4667** | 2256 | 1187 | 663 |
| | Matching rate /% | 17 | 22 | 24 | 24 | **27** | 23 | 19 | 16 |
| | Time /s | 52.46 | 13.27 | 6.36 | 3.84 | **2.06** | 1.35 | 1.08 | 0.43 |

CPU, and 8GB RAM. We quantitatively and qualitatively compare our feature detection and matching results with the most commonly used traditional algorithms, including SIFT [8] and SURF [11]. And also, the stitching results are compared with excellent stitching algorithms including improved SURF [12], APAP [13], SPHP [14], and AANAP [15].

The performance of the proposed method was evaluated by experiments related to image stitching, and the values of each parameter during image processing were counted for data analysis. The methods and experiments were designed and conducted using MATLAB R2017b.

### B. DOWN SAMPLING FACTORS SELECTION

To obtain a more desirable number of feature points and matching rate, the k-value is needed for continuous improvements during experiments. According to different coefficients (K), some remote sensing images of farmlands are selected randomly for experimental analysis. As shown in Table 1, the larger the k-value of k, the smaller the number of feature points and the shorter the time. However, when k = 5, the number of feature points meets the stitching requirement, and the running time meets the fast-stitching requirement and the highest matching rate. Therefore, k = 5 satisfies the research requirements herein.

### C. EXPERIMENTAL RESULTS

### 1) FEATURE DETECTION AND MATCHING COMPARISON ANALYSIS

To verify the alignment effect of the method herein, experiments were conducted as shown in Figures 6, 7, and 8, and different splicing algorithms were compared. The results are shown (a) the traditional SIFT [8], (b) the SURF [11], and
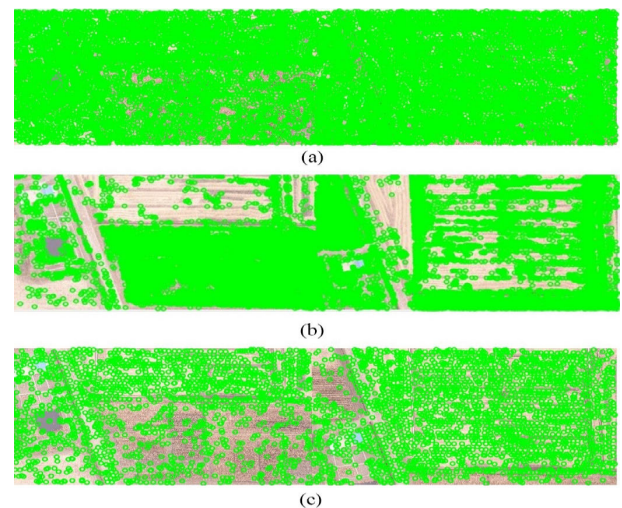


**FIGURE 6.** The feature point detection results of group 1: (a) The result of traditional SIFT [8]; (b) The result of SURF [11]; (c) The result of proposed method.

(c) the proposed method. As can be seen from the Figure, the traditional SIFT [8] algorithm generated too many feature points, which seriously affected the detection and matching efficiency. The SURF [11] algorithm generated fewer feature points, but the feature points are unevenly distributed, thereby affecting the matching accuracy. The algorithm used herein achieved excellent effects: the number of feature points was significantly reduced, and the distribution of feature points was uniform and effective, which finally improved the detection and matching efficiency.

Also, the results of multiple experiments of the three algorithms were counted, and the results are shown in Table 2.

| Method | Number of feature points | | | Number of Matching points | | | Matching rate/% | Time/s |
|---|---|---|---|---|---|---|---|---|
| | Maximum | Average | Minimum | Maximum | Average | Minimum | | |
| SIFT [8] | 59965 | 55230 | 48524 | 8705 | 8366 | 7652 | 15.15 | 69.32 |
| SURF [11] | 15070 | 13644 | 12672 | 1107 | 930 | 565 | 6.82 | 3.11 |
| Proposed method | **6165** | **5707** | **5529** | **1578** | **1266** | **1024** | **22.18** | **2.32** |
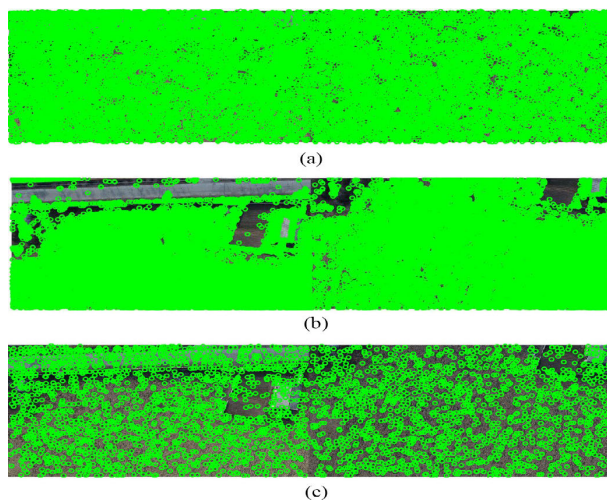


**FIGURE 7.** The feature point detection results of group 2: (a) The result of traditional SIFT [8]; (b) The result of SURF [11]; (c) The result of proposed method.
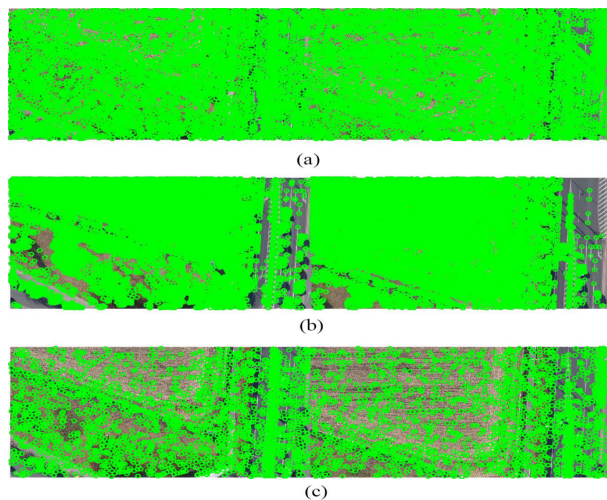


**FIGURE 8.** The feature point detection results of group 3: (a) The result of traditional SIFT [8]; (b) The result of SURF [11]; (c) The result of proposed method.

From the results shown in Table 2, the algorithm used in this study detected the least number of feature points and reduced 90% and 58% of the feature points compared with the traditional SIFT [8] and SURF [11] algorithms, respectively. The matching efficiency (matching efficiency is the ratio of the average number of matching points to the average number of feature points) is 22.18%, which was the highest among the three algorithms. The running time of the three algorithms shows that the algorithm proposed herein took the least time, and without affecting the splicing accuracy, it saved 97% and 25% of the time taken by the traditional SIFT [8] and SURF [11] algorithms, respectively, which greatly improved the efficiency of feature detection and matching and achieved fast detection.

### 2) ROBUSTNESS COMPARISON ANALYSIS

To verify the robustness of the algorithm to image rotation, three algorithms test the image rotation by eight angles, respectively, and the matching effect and test results are shown in Figure 9.

As shown in Figure 9, the algorithm proposed herein has good stability in rotational transformation because the number of feature points extracted was significantly lower than that extracted by the standard SIFT [8] and SURF [11] algorithms, which changed insignificantly in the case of image rotation. Furthermore, in the case of image rotation, it also maintained good and stable matching performance. Therefore, it has higher robustness for rotated image stitching.

### 3) MATCHING RESULT OPTIMIZATION ANALYSIS

The PROSAC algorithm is used to optimize the fast-matching results of the three algorithms, the comparison results are shown in Figure 10. It can be seen that, after the calculation and optimization, the false matches among them are removed to get the inner points (correct matching points). The algorithm in this study had the highest inside point rate (percentage of correctly matched points) of about 95%, the SIFT [8] algorithm is about 92%, and the SURF [11] algorithm is about 89%.

The fine-matching runtime results for the three algorithms are listed in Table 3. According to Table 3, the algorithm in this study dramatically reduces the running time and significantly improves the stitching efficiency.

**TABLE 3.** Running time statistics.

| Group number | Time/s | | |
|---|---|---|---|
| | SIFT [8] | SURF [11] | Proposed method |
| 1 | 31.34 | 10.28 | **3.82** |
| 2 | 38.28 | 12.57 | **3.88** |
| 3 | 32.84 | 11.36 | **2.66** |
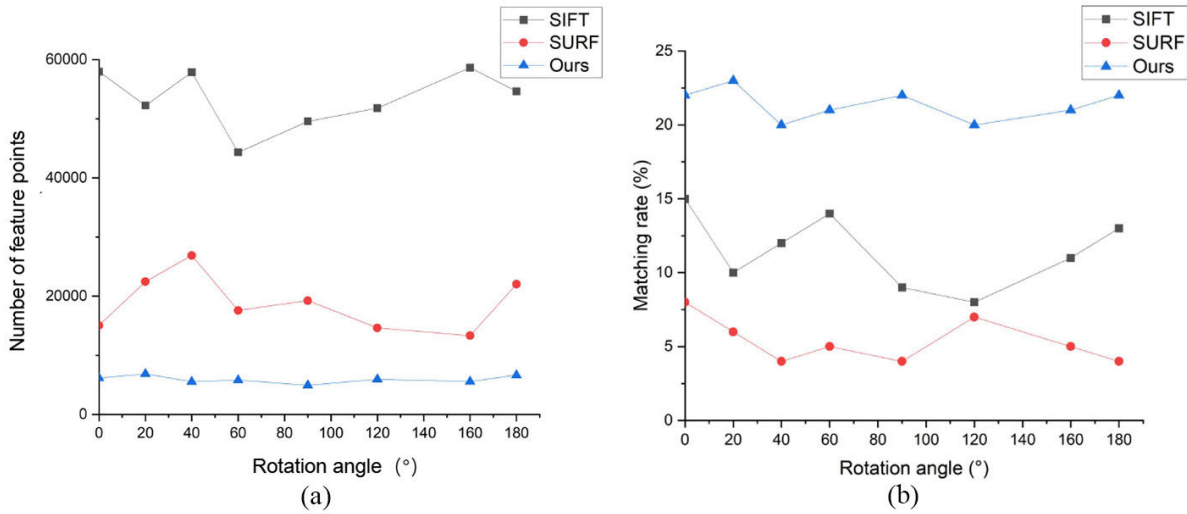
**FIGURE 9.** Rotational robustness comparison chart, (a) Feature point detection line chart; (b) Feature matching rate line chart.
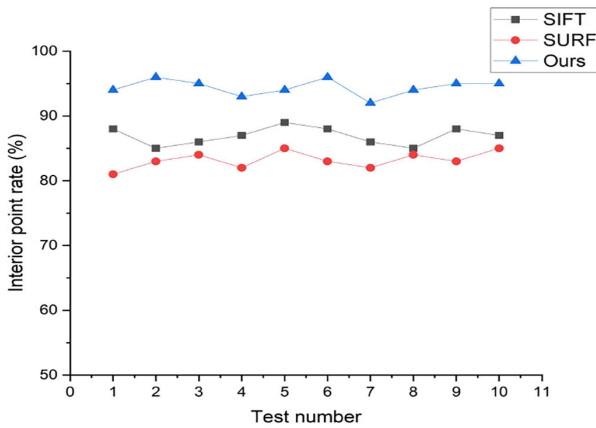


**FIGURE 10.** A comparison chart of precision matching results.

#### 4) EVALUATION CRITERIA

Two methods were used to evaluate the image quality: first, a subjective evaluation, in which the panoramic image quality is evaluated by subjective visual effects. The second is an objective evaluation, in which information entropy (IE) [28], mean gradient (Clarity) [29], and image contrast (IC) are selected as objective evaluation indices, as follows:

$$IE = -\sum_{I=0}^{L-1} [P_f(i) \log_2 p_f(i)] \tag{17}$$

where f is the image, $P_f$ is the proportion of all pixels with a gray value i in the overall image, L is the gray level, and 256 gray levels are generally selected for the statistics.

$$Clarity = \sum_{y} \sum_{x} |f(x+2, y) - f(x, y)|^2 \tag{18}$$

where f(x,y) is the gray value of the image f corresponding to a pixel (x,y) and Clarity is the result of Image clarity calculation.

$$IC = \sum_{\delta} \delta(i, j)^2 P_\delta(i, j) \tag{19}$$

where $\delta(i, j) = |i - j|$, the grayscale difference between adjacent pixels: $P_\delta(i, j)$ is the pixel distribution probability of the grayscale difference $\delta$ between adjacent pixels.

#### 5) TWO-IMAGE STITCHING RESULTS ANALYSIS

The image of the straw farmland had a more complex background, which contained roads, houses, straw with obvious grain characteristics, etc. A comparison of the stitching result of the above three groups of images between the proposed method and some excellent stitching algorithms respectively is presented in Figures 11, 12, and 13 where the details of the image are zoomed in, shown by the corresponding red boxes in the mosaic images. In the result of (a) SURF [12], it is seen that there was a clear overlap and misalignment in the figure. A similar result for blurring and misalignment phenomena were also observed in the output of (b) APAP [13], and (c) SPHP [14]. The output of (d) AANAP [14] shows a significant line in the stitching area. The proposed method achieved good stitching results with no blurring and misalignment phenomena; and had a natural and clear transition in the stitching area.

Table 4 respectively shows the information entropy, mean gradient, and image contrast of the five methods in three groups of images, where the best performance is highlighted in bold. In Table 4, the proposed method significantly outperformed other methods in multiple sets of experiments. And it has a large improvement in stitching time compared to other methods, significantly improving stitch efficiency and meeting the need for rapid stitching.

#### 6) MULTI-IMAGE STITCHING RESULTS ANALYSIS

The following Figure 14 shows the panoramic stitching image (Figure 15) of the stitching results of each layer
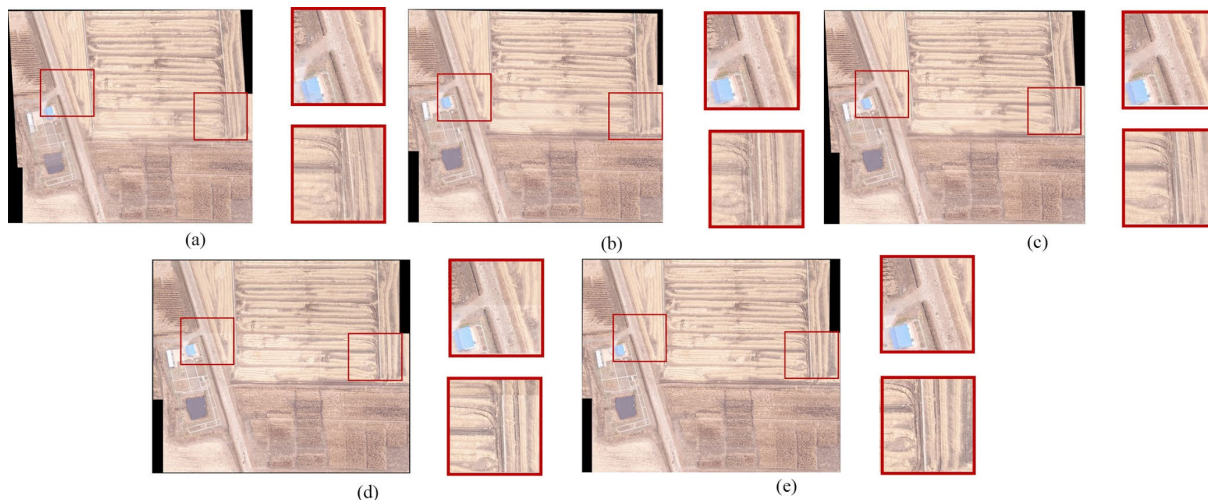
**FIGURE 11.** Comparison of image stitching results of group 1: (a) SURF [12], (b) APAP [13], (c) SPHP [14], (d) AANAP [15], and (e) the proposed method. The highlighted red boxes in each image are zoomed in (shown by the corresponding boxes on the right) for a detailed visual comparison frame that highlights the details of the image.
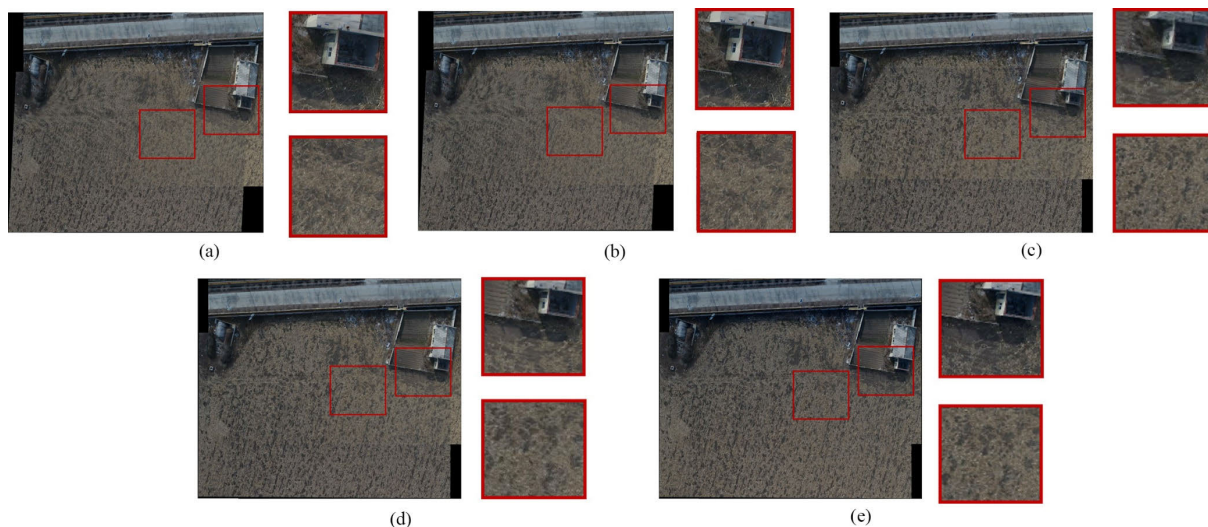


**FIGURE 12.** Comparison of image stitching results of group 2: (a) SURF [12], (b) APAP [13], (c) SPHP [14], (d) AANAP [15], and (e) the proposed method. The highlighted red boxes in each image are zoomed in (shown by the corresponding boxes on the right) for a detailed visual comparison frame that highlights the details of the image.

**TABLE 4.** Evaluation indicators comparison with excellent stitching algorithms.

| Group number | Evaluation Indicators | SURF [12] | APAP [13], | SPHP [14] | AANAP [15] | proposed method |
|---|---|---|---|---|---|---|
| 1 | IE | 6.71 | 6.73 | 6.75 | 6.78 | **6.83** |
| | Clarity | 5.76 | 5.82 | 5.99 | 6.02 | **6.13** |
| | IC | 125.74 | 132.21 | 136.62 | 141.62 | **144.23** |
| | Time/s | 44.29 | 334.27 | 322.13 | 289.45 | **14.06** |
| 2 | IE | 6.69 | 6.74 | 6.76 | 6.83 | **6.94** |
| | Clarity | 3.42 | 3.58 | 3.90 | 3.96 | **4.54** |
| | IC | 53.94 | 54.76 | 55.63 | 56.23 | **73.24** |
| | Time/s | 48.37 | 352.13 | 344.54 | 314.92 | **15.68** |
| 3 | IE | 7.34 | 7.35 | 7.36 | 7.38 | **7.52** |
| | Clarity | 9.23 | 9.25 | 9.27 | 9.33 | **10.45** |
| | IC | 294.15 | 298.34 | 299.94 | 304.75 | **377.23** |
| | Time/s | 36.81 | 329.74 | 289.39 | 253.94 | **10.36** |
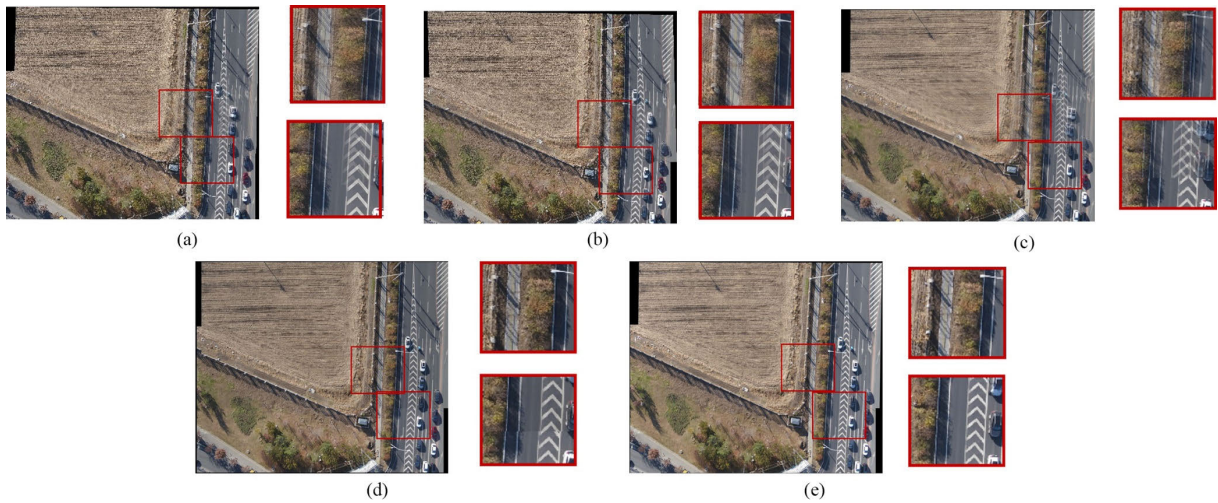
**FIGURE 13.** Comparison of image stitching results of group 3: (a) SURF [12], (b) APAP [13], (c) SPHP [14], (d) AANAP [15], and (e) the proposed method. The highlighted red boxes in each image are zoomed in (shown by the corresponding boxes on the right) for a detailed visual comparison frame that highlights the details of the image.

**TABLE 5.** Evaluation results of objective indicators.

| Group number | Traditional method | | | | Proposed method | | | |
|---|---|---|---|---|---|---|---|---|
| | IE | Clarity | IC | Time/s | IE | Clarity | IC | Time/s |
| 1 | 6.23 | 6.13 | 121.53 | 12563.58 | **6.83** | **6.74** | **137.35** | **883.21** |
| 2 | 6.29 | 6.24 | 123.49 | 12364.41 | **6.86** | **6.81** | **138.26** | **786.34** |
| 3 | 6.18 | 6.14 | 121.64 | 12401.35 | **6.78** | **6.79** | **136.82** | **792.61** |
| 4 | 6.26 | 7.05 | 288.34 | 12577.24 | **6.88** | **7.42** | **309.05** | **889.23** |
| 5 | 6.24 | 7.18 | 286.73 | 12284.26 | **6.76** | **7.46** | **319.64** | **816.23** |
| 6 | 6.20 | 7.23 | 309.62 | 12326.72 | **6.65** | **7.59** | **3426.2** | **786.23** |
| 7 | 6.48 | 6.34 | 237.23 | 11877.36 | **7.15** | **8.56** | **288.73** | **779.81** |
| 8 | 6.32 | 6.47 | 249.83 | 12232.26 | **7.22** | **8.67** | **291.22** | **806.76** |
| 9 | 6.57 | 6.53 | 256.53 | 12527.22 | **7.75** | **8.76** | **294.56** | **836.53** |
| 10 | 6.31 | 6.26 | 125.31 | 12566.38 | **6.88** | **6.82** | **138.61** | **826.86** |
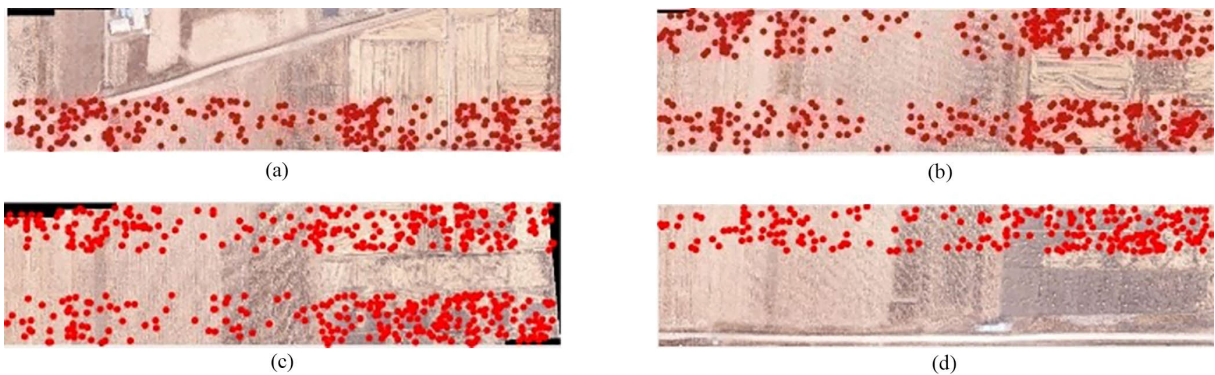


**FIGURE 14.** Layered stitching results. (a) The image stitching results of layer 1; (b) The image stitching results of layer 2; (c) The image stitching results of layer 3; (d) The image stitching results of layer 4.

generated according to the method proposed herein. As shown in Figures 15, 16, and 17, three groups of different methods of panoramic stitching results were compared and analyzed.

The subjective evaluation outcome reveals that the stitching results of each layer are more natural, better retaining the detailed components of the image, high definition, and high overall image quality. From the results shown in Figures 15, 16, and 17, the method proposed herein achieved excellent stitching results for all three groups of images with complex backgrounds and large differences in features. The details of the selected image in the red frame are enlarged,
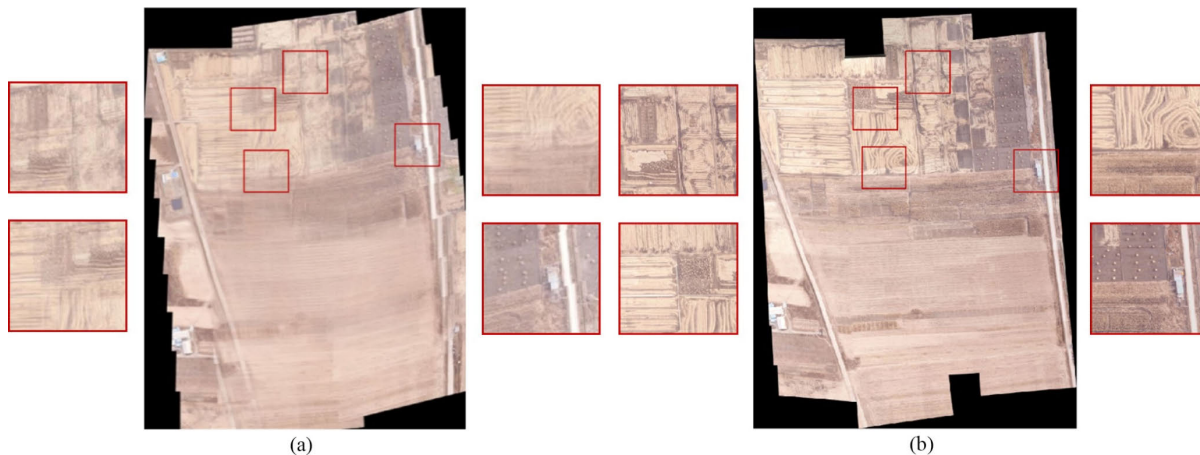
**FIGURE 15.** The panoramic stitching results of group 1: (a) The result of the traditional method; (b) The result of proposed method. The highlighted red boxes in each image are zoomed in for a detailed visual comparison.
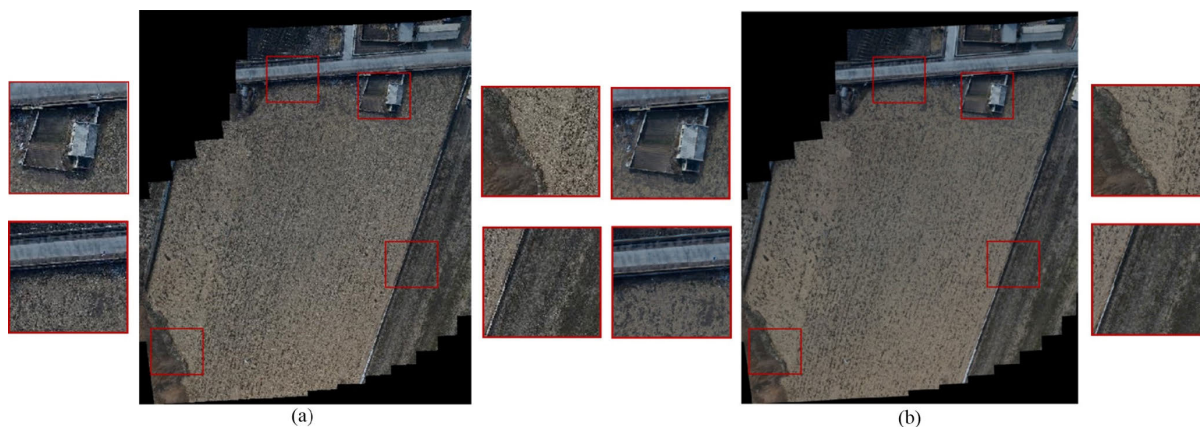


**FIGURE 16.** The panoramic stitching results of group 2: (a) The result of the traditional method; (b) The result of proposed method. The highlighted red boxes in each image are zoomed in for a detailed visual comparison.
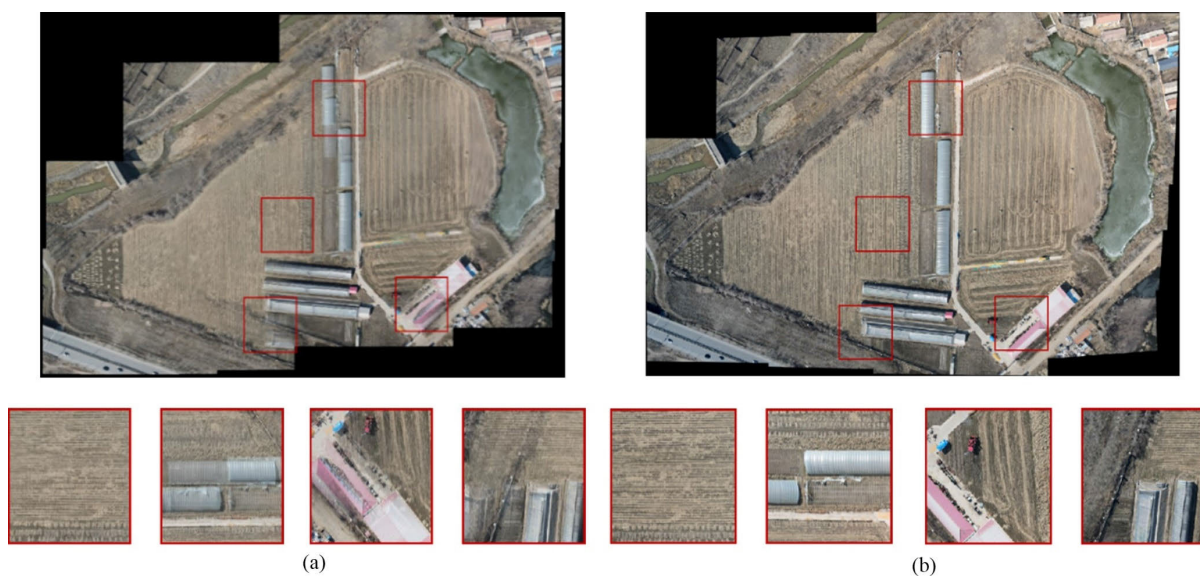


**FIGURE 17.** The panoramic stitching results of group 3: (a) The result of the traditional method; (b) The result of proposed method. The highlighted red boxes in each image are zoomed in for a detailed visual comparison.
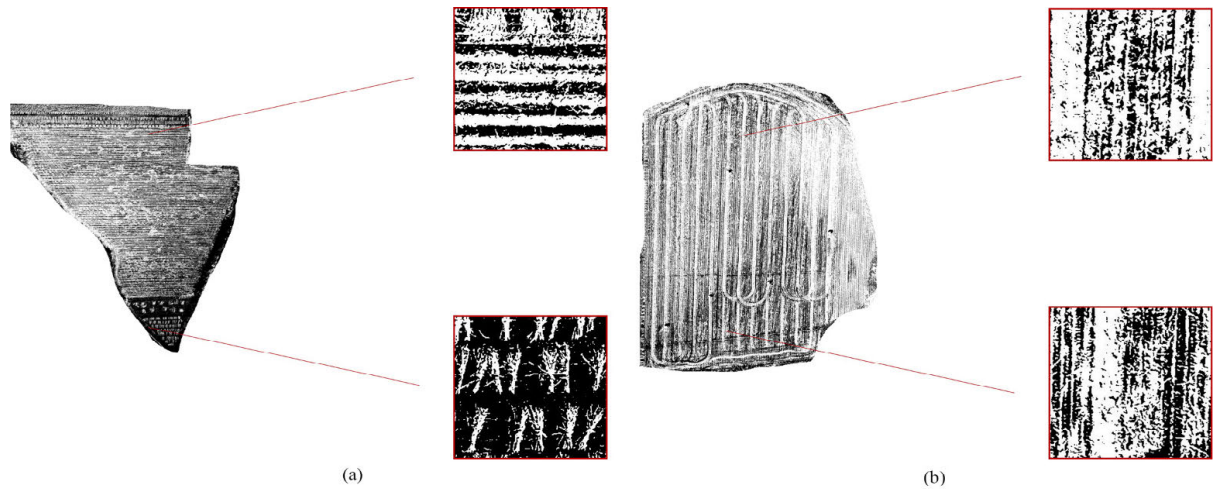
**FIGURE 18.** Segmentation results for two-threshold; (a) Segmentation results for Parcel 1; (b) Segmentation results for Parcel 2. The red frame highlights the details of the image.
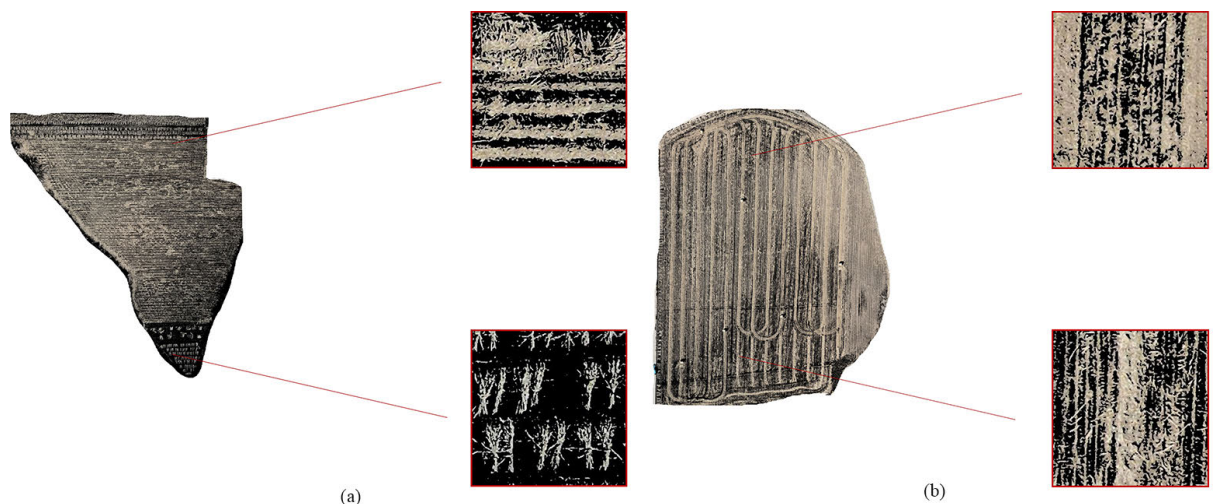


**FIGURE 19.** Segmentation results for multi-threshold; (a) Segmentation results for Parcel 1; (b) Segmentation results for Parcel 2. The red frame highlights the details of the image.

and evidently, the overall quality of the image stitched by the method proposed herein is high, the details are clear, the stitching effect is natural, and there is no missing stitching and ghosting phenomenon. However, the overall image quality of the stitched image of the traditional method is low, with obvious ghosting, misalignment, and blurring effects. The objective evaluation indices of the two methods were also calculated, and the results are shown in Table 5.

From the results shown in Table 5, after several sets of experiments, IE [26], Clarity [27], and IC of the method proposed herein were significantly higher, with better image quality. According to the subjective and objective index evaluations, the stitching quality of the method herein is high, which can improve the clarity and fusion effect of the stitching image and solve the misalignment and ghosting problems caused by the traditional method.

## IV. APPLICATIONS

Currently, the flexible characteristics of UAVs are used to acquire images, and a complete image of the area to be measured is obtained by the image-stitching technique. Afterward, the image is processed simply and easily by machine vision techniques using image segmentation. This approach can provide an image and methodological basis for calculating straw cover [28] and monitoring crop growth.

The DE-AS-MOGWO [29] algorithm was used to perform two-threshold and multi-threshold segmentation on the panoramic images herein, respectively, and the result graphs are shown in Figures 18 and 19. The straw coverage area and rate of the segmented map plots were calculated using pixel points and compared with the manual segmentation results of Photoshop software to judge the accuracy and validity of the

| Method | Parcel 1 | | | Parcel 2 | | |
|---|---|---|---|---|---|---|
| | Straw covered area | Parcel area | Straw coverage rate | Straw covered area | Parcel area | Straw coverage rate |
| Manual segmentation | $2797/m^2$ | $3028m^2$ | 92.37% | $2265m^2$ | $2536m^2$ | 89.31% |
| Algorithm segmentation | $2729m^2$ | $3028m^2$ | 90.12% | $2196m^2$ | $2536m^2$ | 86.59% |

information after the panoramic image segmentation, and the results are statistically analyzed as shown in Table 6.

As shown in Figures 18, and 19, the segmentation result was accurate, with obvious straw coverage, clear and complete straw, no obvious mis-segmentation, and high image quality.

From the results shown in Table 6, the generated panoramic stitching map obtained by the method proposed herein has high quality and complete image information, which can provide data support for the subsequent segmentation and straw coverage calculation. Furthermore, the straw coverage calculation error after segmentation is within 3%, which can meet the demand for large area detection of straw coverage and provide a reference for straw coverage detection, which has paramount practical significance.

## V. CONCLUSION

The method used herein is based on remote sensing data of straw farmlands collected by UAV. Such an approach uses image-stitching technology to generate high-resolution farmland area images, providing large-scale and large-area image information for straw cover and geographic information detection. Herein, a fast-stitching method based on an improved SIFT algorithm for farmland aerial images was proposed, which quickly and accurately extracts straw target feature points from high-resolution images collected by the UAV aerial photography under complex background conditions. Furthermore, it distinguishes between straw and other sources of interference such as clutter in the feature matching stage for accurate matching of matching points, accurately calculates the conversion model, enables a certain degree of fusion improvement of the stitched images, and improves image quality, thereby realizing panoramic stitching of straw farmland images. The results of the experiments conducted using this method are as follows:

(1) In the feature extraction stage, the algorithm down samples the high-resolution image, reduces a large number of feature points, uses MN-SIFT feature descriptors, and effectively improves the efficiency of feature point detection, compared with the traditional SIFT algorithm and SURF algorithm, the number of feature points is reduced by 90% and 58%; the running time is reduced by 97% and 25%, achieving fast detection.

(2) In the feature matching stage, the algorithm recovers feature point coordinates and scale parameters to ensure image accuracy, and matches through MN-SIFT feature descriptors with a matching efficiency of 22.18%, which is significantly higher than the traditional SIFT algorithm and

SURF algorithm. The PROSAC algorithm eliminates 5% of mismatches and accurately calculates the transformation model to improve the image stitching accuracy.

(3) The combination of the optimal stitching line and fade in and out method effectively removes ghosting and misalignment in the stitched images, avoids image information loss, and preserves the integrity of image detail information. The method in this paper achieves a good fusion effect and high quality in the stitching of two images, and the performance of the method is better than other widely used excellent methods compared with other stitching methods.

(4) For multi-image stitching of high-resolution straw images, a layered stitching strategy of multiple high-resolution remote sensing images is designed to generate high-quality panoramic stitched images. The panoramic image generated by this method is significantly better than the traditional method by subjective and objective evaluation, reduces the error accumulated by successive matrix multiplication, eliminates the blurring and misplacing generated by multi-image stitching, and improves the accuracy of image stitching.

(5) The panoramic stitching map generated in this paper has high quality, which can provide data support for the subsequent segmentation and straw coverage calculation, and the experimental error is less than 5%, which has accuracy and validity.

Our fast stitching method can be used in the field of remote sensing and agricultural monitoring. The further work scope of the research includes extending the image stitching function to UAVs to achieve real-time automatic stitching of UAVs and generation of real-time panoramic images for crop assessment and prediction through AI and machine learning techniques for analysis of large panoramic image datasets of agricultural fields. The current UAV multispectral technology is developing rapidly, and the application of image stitching technology to the stitching of each frequency band of multi-spectral is also very worth studying.

### REFERENCES

[1] P. Wang, X. W. Luo, Z. Y. Zhou, Y. Zang, and L. Hu, "An overview of key technologies for remote sensing information acquisition based on micro and small UAVs," *J. Agricult. Eng.*, vol. 30, no. 18, pp. 1–12, Sep. 2014.

[2] M. A. Haq, "CNN based automated weed detection system using UAV imagery," *Comput. Syst. Sci. Eng.*, vol. 42, no. 2, pp. 837–849, 2022.

[3] A. Attaallah and R. A. Khan, "SMOTEDNN: A novel model for air pollution forecasting and AQI classification," *Comput., Mater. Continua*, vol. 71, no. 1, pp. 1403–1425, 2022.

[4] M. A. Haq, "CDLSTM: A novel model for climate change forecasting," *Comput., Mater. Continua*, vol. 71, no. 2, pp. 2363–2381, 2022.

[5] M. A. Haq, "Planetscope nanosatellites image classification using machine learning," *Comput. Syst. Sci. Eng.*, vol. 42, no. 3, pp. 1031–1046, 2022.

[6] Y. L. Bai, L. P. Yang, L. Wang, Y. L. Lu, and H. Wang, "Low-altitude remote sensing technology for agriculture and its application prospects," *Agricult. Netw. Inf.*, vol. 24, no. 1, pp. 5–7, Jan. 2010.

[7] M. A. Haq, G. Rahaman, P. Baral, and A. Ghosh, "Deep learning based supervised image classification using UAV images for forest areas classification," *J. Indian Soc. Remote Sens.*, vol. 49, no. 3, pp. 601–606, Mar. 2021.

[8] K. X. Wang, Q. Fu, Z. H. Zhang, X. Jiang, and Z. J. Hao, "Effects of straw mulching and topsoil tillage on soil environment in the root zone of northeastern black soil," *J. Agricult. Machinery*, vol. 47, no. 3, pp. 131–137, Jan. 2016.

[9] D. G. Lowe, "Distinctive image features from scale-invariant keypoints," *Int. J. Comput. Vis.*, vol. 60, no. 2, pp. 91–110, Mar. 2004.

[10] T. Y. Hong, H. J. You, and X. Sun, "Automatic stitching method of UAV images with satellite images as the base map," *Mapping Sci.*, vol. 40, no. 6, pp. 11–16, Apr. 2015.

[11] H. T. Bay Tuytelaars and L. V. Gool, "SURF: Speeded up robust features," in *Proc. Eur. Conf. Comput. Vis. (ECCV)*, Graz, Austria, Sep. 2006, pp. 404–417.

[12] T. X. Hu, X. F. Niu, Y. Tan, and X. P. Chen, "UAV remote sensing image stitching technology based on surf algorithm," *Mapping Bull.*, vol. 60, no. 1, pp. 55–58, Jan. 2015.

[13] J. Zaragoza, T.-J. Chin, M. S. Brown, and D. Suter, "As-projective-as-possible image stitching with moving DLT," in *Proc. IEEE Conf. Comput. Vis. Pattern Recognit.*, Portland, OR, USA, Jun. 2013, pp. 2339–2346.

[14] C.-H. Chang, Y. Sato, and Y.-Y. Chuang, "Shape-preserving half-projective warps for image stitching," in *Proc. IEEE Conf. Comput. Vis. Pattern Recognit.*, Columbus, OH, USA, Jun. 2014, pp. 3254–3261.

[15] C.-C. Lin, S. U. Pankanti, K. N. Ramamurthy, and A. Y. Aravkin, "Adaptive as-natural-as-possible image stitching," in *Proc. IEEE Conf. Comput. Vis. Pattern Recognit. (CVPR)*, Boston, MA, USA, Jun. 2015, pp. 1155–1163.

[16] J. B. Yang, Y. T. Jang, X. B. Yang, and G. M. Guo, "A fast stitching method for UAV images based on dense sift features," *J. Geoinformation Sci.*, vol. 21, no. 4, pp. 588–599, Apr. 2019.

[17] H. Wu and L. Jin, "Rapid stitching technology for multi-scene high-resolution remote sensing images," *Flight Control Detection*, vol. 4, no. 5, pp. 62–70, Sep. 2021.

[18] X. Wei, W. Yan, Q. Zheng, M. Gu, K. Su, G. Yue, and Y. Liu, "Image redundancy filtering for panorama stitching," *IEEE Access*, vol. 8, pp. 209113–209126, 2020.

[19] N. T. Pham, S. Park, and C.-S. Park, "Fast and efficient method for large-scale aerial image stitching," *IEEE Access*, vol. 9, pp. 127852–127865, 2021.

[20] T. Zhang, R. Zhao, and Z. Chen, "Application of migration image registration algorithm based on improved SURF in remote sensing image mosaic," *IEEE Access*, vol. 8, pp. 163637–163645, 2020.

[21] L. Deng, X. Yuan, C. Deng, J. Chen, and Y. Cai, "Image stitching based on nonrigid warping for urban scene," *Sensors*, vol. 20, no. 24, p. 7050, Dec. 2020.

[22] S. Saleem, A. Bais, and R. Sablatnig, "Towards feature points based image matching between satellite imagery and aerial photographs of agriculture land," *Comput. Electron. Agricult.*, vol. 126, pp. 12–20, Aug. 2016.

[23] J. Lu, Y. Xu, and Z. Gao, "An improved method of an image mosaic of a tea garden and tea tree target extraction," *AgriEngineering*, vol. 4, no. 1, pp. 231–254, Feb. 2022.

[24] R. J. Al-Azawi, N. M. G. Al-Saidi, H. A. Jalab, R. W. Ibrahim, and D. Baleanu, "Image splicing detection based on texture features with fractal entropy," *Comput., Mater. Continua*, vol. 69, no. 3, pp. 3903–3915, 2021.

[25] Z. Wang, J. Li, X. Wang, and X. Niu, "Underwater terrain image stitching based on spatial gradient feature block," *Comput., Mater. Continua*, vol. 72, no. 2, pp. 4157–4171, 2022.

[26] Y. Sen, J. H. Zhu, H. Liu, Y. M. Cui, and B. N. Zhang, "Fast switching of plant images based on color and depth information combined with a K-means clustering algorithm," *J. Agricult. Eng.*, vol. 34, no. 23, pp. 134–141, Dec. 2018.

[27] X. Wang, J. F. Ning, Y. X. Cao, and W. T. Han, "UAV remote sensing image stitching technology based on sifting algorithm," *J. Jilin Univ.*, vol. 35, no. 2, pp. 188–197, Mar. 2017.

[28] Y. Y. Liu, Y. Y. Wang, H. Y. Yu, M. X. Qin, and J. H. Sun, "Straw cover detection based on multi-threshold image segmentation algorithm," *J. Agricult. Machinery*, vol. 49, no. 12, pp. 27–35, Dec. 2018.

[29] Y. Y. Liu, J. H. Sun, S. J. Zhang, H. Y. Yu, and Y. Y. Wang, "Detection of straw cover with multi-threshold multi-objective UAV image segmentation optimization algorithm," *J. Agricult. Eng.*, vol. 36, no. 20, pp. 134–143, Oct. 2020.

**YUANYUAN LIU** was born in Jilin, Changcun, China, in 1980. She received the Ph.D. degree from Jilin University, China. She is currently a Visiting Scholar at Oklahoma State University, USA. She is also a Lecturer with Jilin Agricultural University and a master's degree Advisor. Her research interests include the area of image and video signal processing.

**MING HE** was born in Jilin, China, in 1999. He is currently pursuing the master's degree with the School of Information Technology, Jilin Agricultural University. His research interests include image processing and computer vision.

**YUEYONG WANG** was born in Jilin, Changcun, China, in 1979. He received the Ph.D. degree from Jilin University, China. He is currently an Associate Professor with Jilin Agricultural University and a master's degree Advisor. He is also a Visiting Scholar at the Technical University of Dresden, Germany. His research interests include intelligent systems, bioenvironmental, and energy engineering.

**YU SUN** was born in Liaoning, China. She is currently pursuing the master's degree with the School of Information Technology, Jilin Agricultural University. Her research interests include image processing and computer vision.

**XUEBING GAO** was born in Liaoning, China. She is currently pursuing the master's degree with the School of Information Technology, Jilin Agricultural University. Her research interests include image processing and computer vision.

● ● ●